Supplementary information for "Orbital CO_2 reconstruction using boron isotopes during the late Pleistocene, an assessment of accuracy." By de la Vega et al.

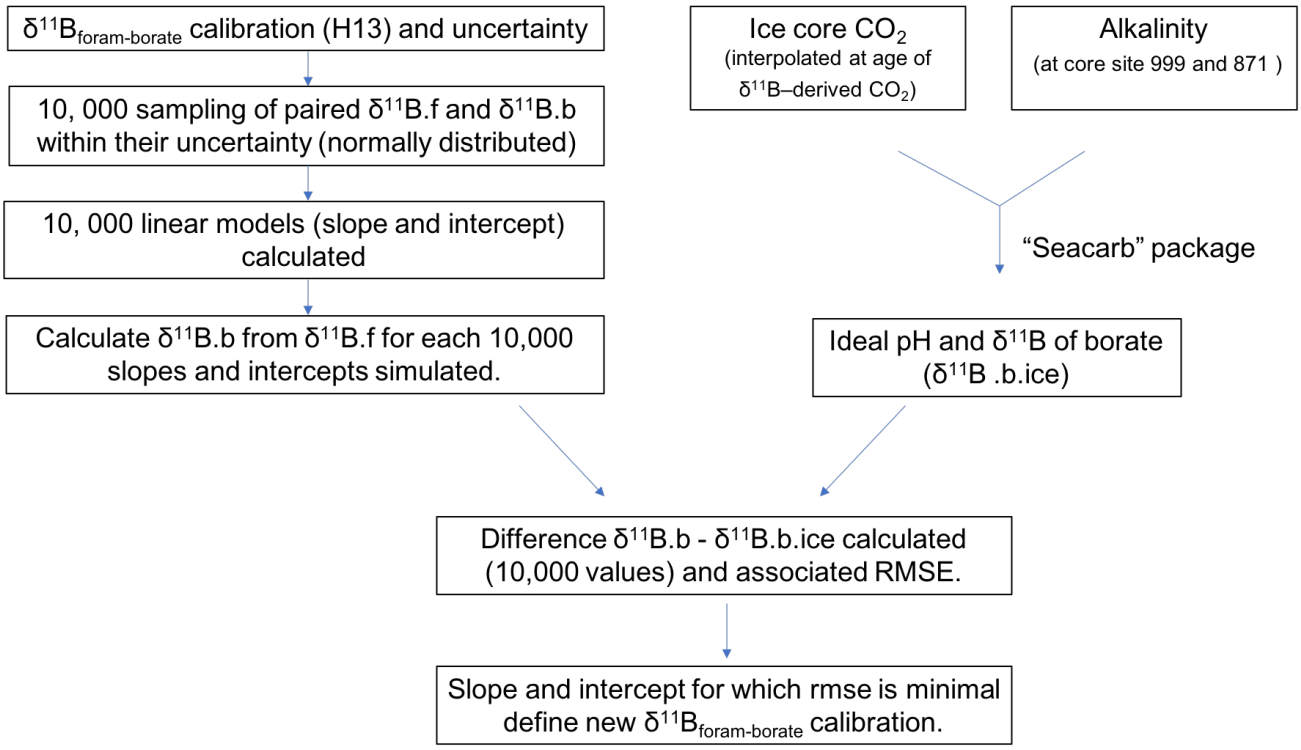

Figure S1. Optimisation of the borate-foram $\delta^{11}B$ calibration by minimising the RMSE between the $\delta^{11}B$ of borate derived from ice core CO_2, and the $\delta^{11}B$ of borate simulated from 10,000 slopes and intercept. The slopes and intercept are simulated within the uncertainty of $\delta^{11}B$ borate and pH calibration of Henehan et al. (2013).

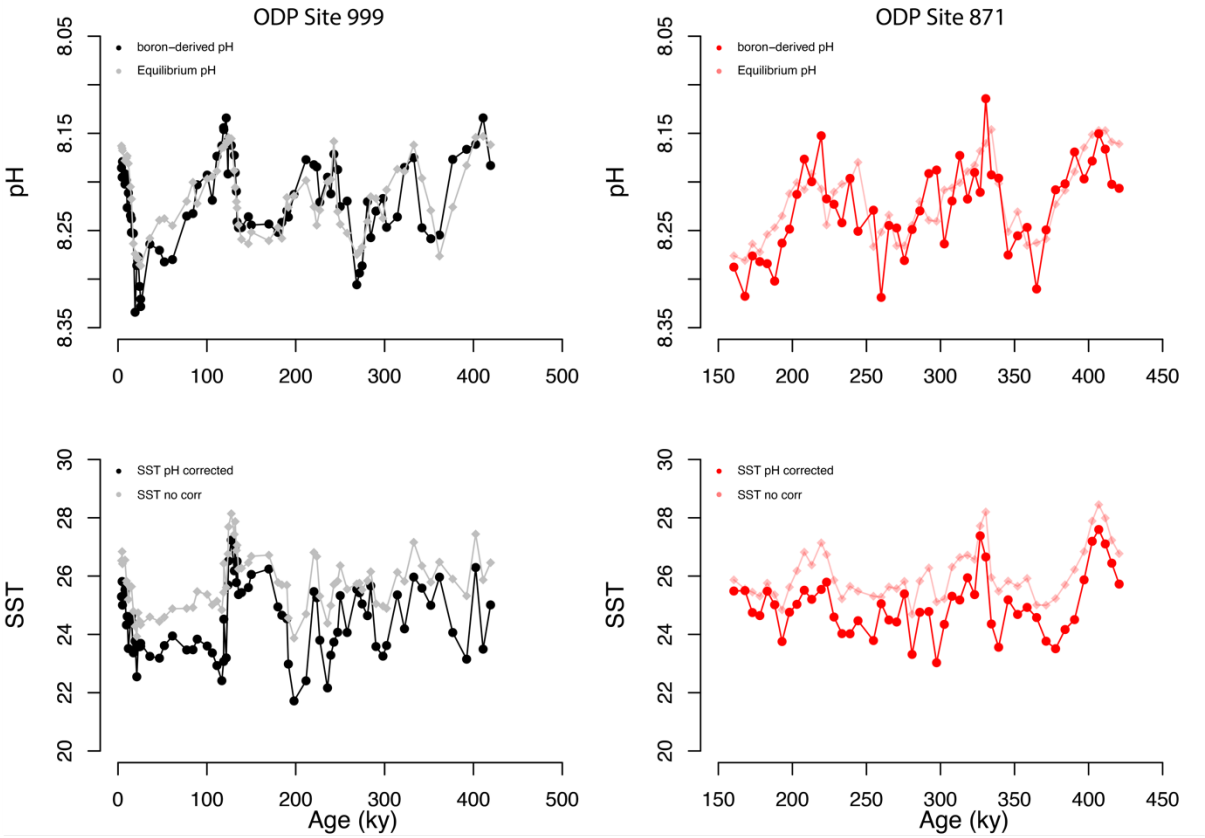

Figure S2. Top row: δ^{11}B-derived pH (black and dark red) and equilibrium pH (i.e. derived from ice core CO_2, grey and light red). Bottom row: Mg/Ca-derived sea surface temperature (SST) with no pH correction (grey and light red) and with pH correction (black and dark red).

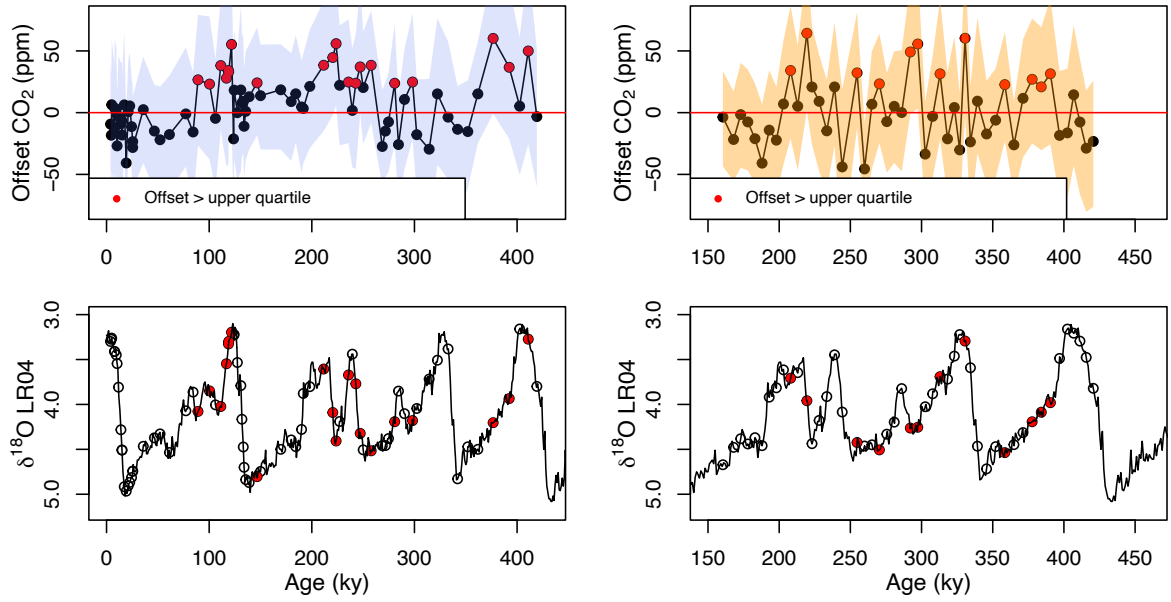

Figure S3. Upper panel: CO_2 offset (δ^{11}B-derived CO_2 minus ice core CO_2), red dots are the offset above the upper quartile (i.e. 25% of the data that lies above the upper quartile). Lower panel: LR04 δ^{18}O (black line), interpolated δ^{18}O (open circles) from the δ^{11}B-derived CO_2 and red points are the interpolated values for which CO_2 offset is high (above the upper quartile). This shows that the values of high CO_2 offset (between boron-derived and ice core CO_2) tend to fall within periods at the beginning of the glaciation. Left panels for ODP Site 999, and right panels for ODP Site 871.

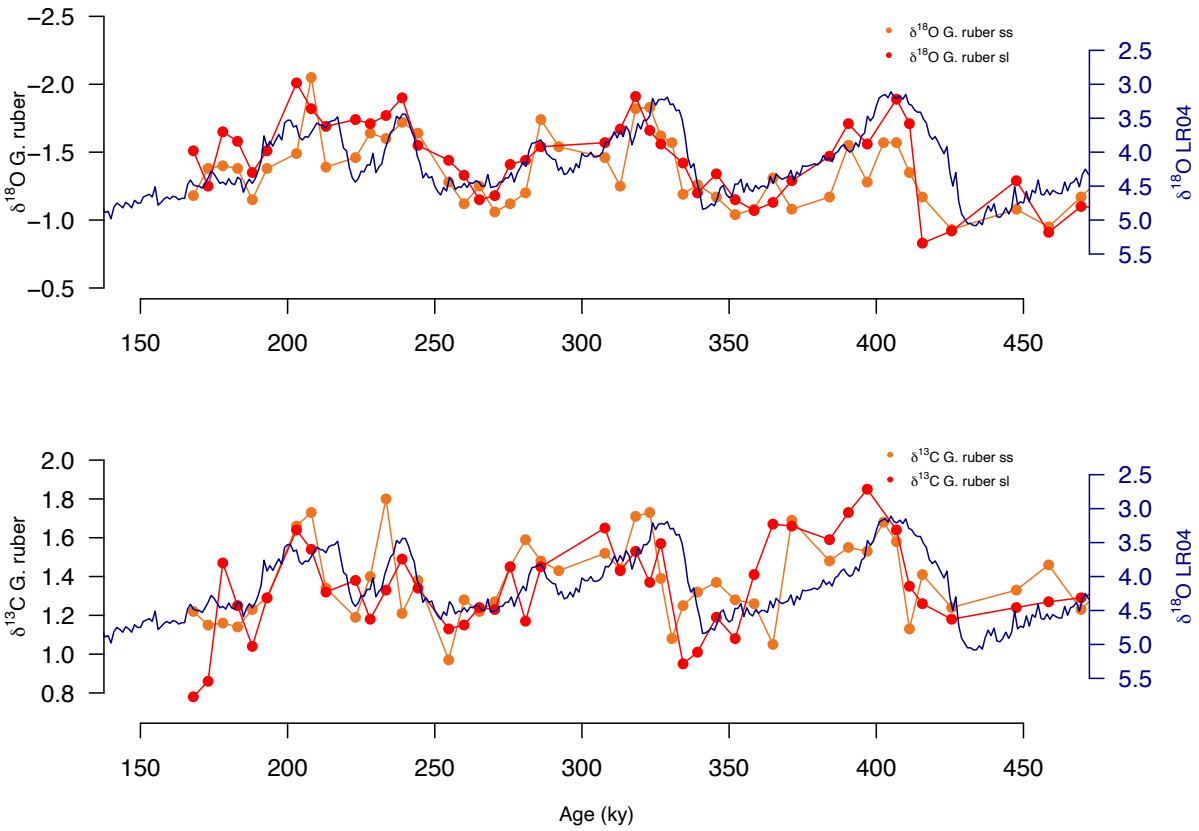

Figure S4. Time series of $\delta^{13}C$ and $\delta^{18}O$ for the two morphotypes of *G. ruber* at ODP Site 871 (sensu stricto, orange; and sensu lato, red). The benthic $\delta^{18}O$ stack LR04 is plotted for reference (dark blue).

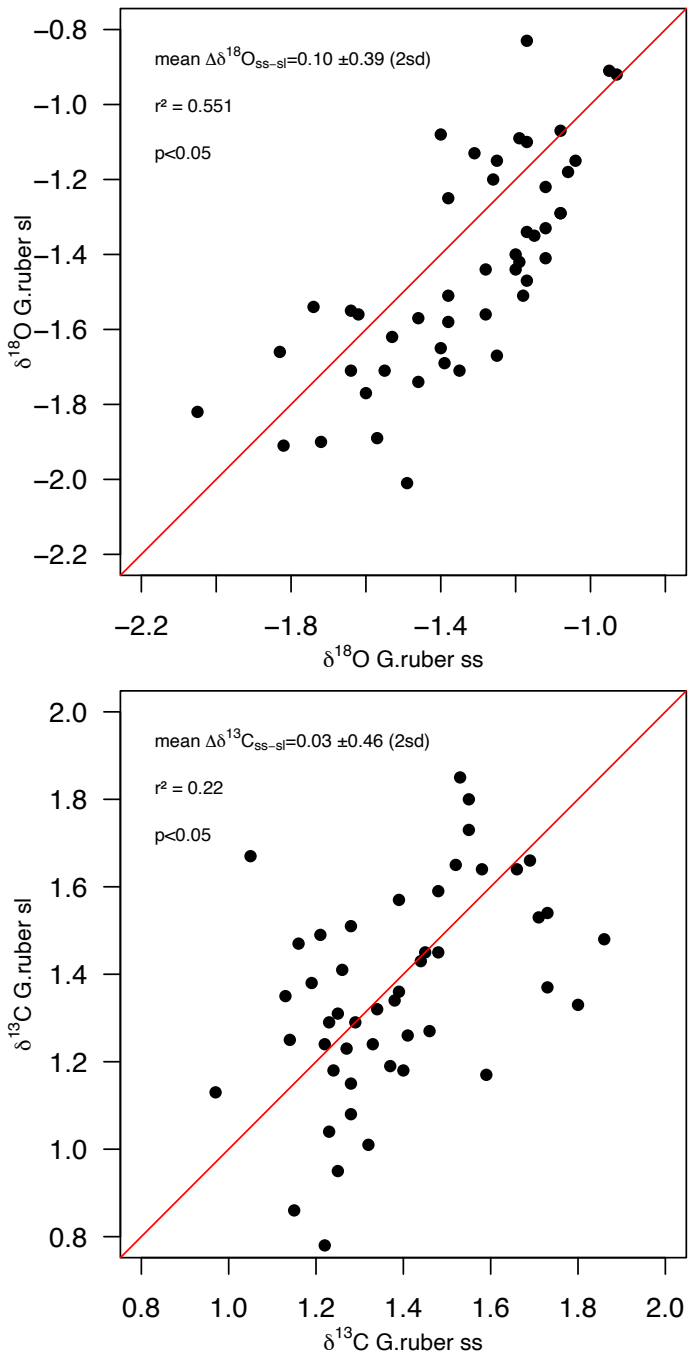

Figure S5. Cross plot of $\delta^{18}O$ and $\delta^{13}C$ of the two morphotypes of *G. ruber* (*sensu stricto* and *sensu lato)* and associated r^2 . The red line is the 1:1 line. The mean offset and 2 standard deviation between $\delta^{18}O$ and $\delta^{13}C$ of both morphotypes is shown (‰).

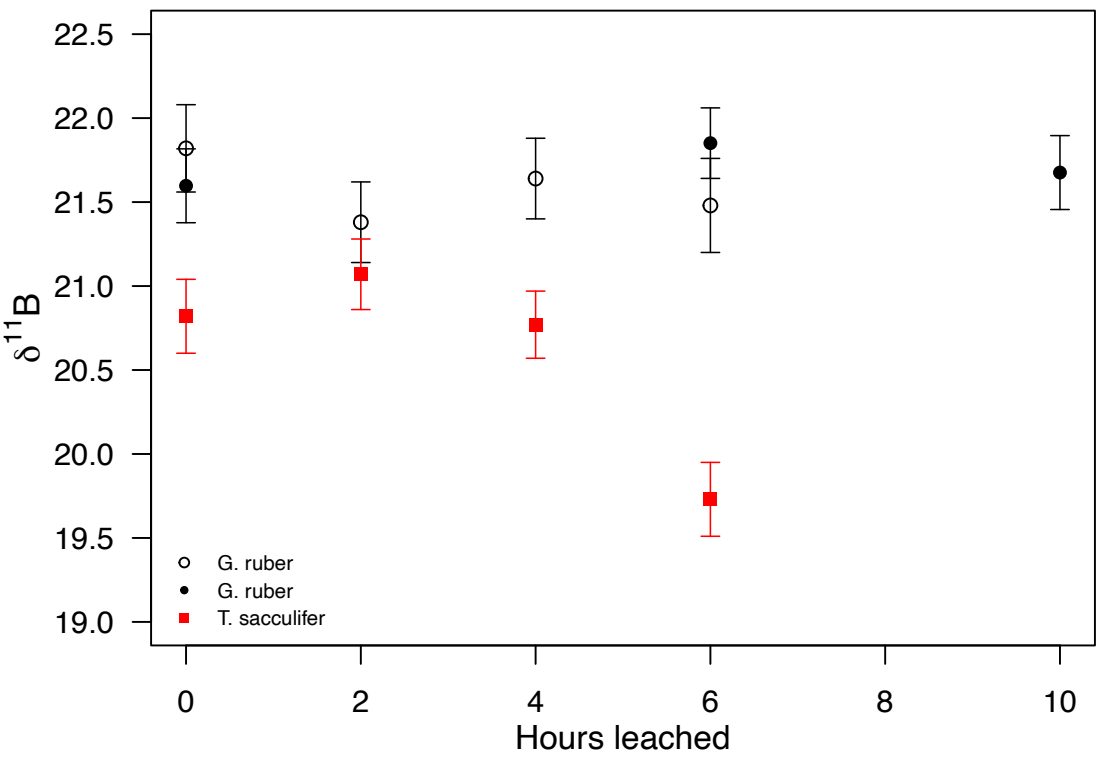

Fig S6. Dissolution tests conducted on *T. sacculifer* (size 500-600 µm) and *G. ruber ss* (size 300-355 µm). Whole foraminifera tests were put in contact with 0.0001M HNO_3 (pH 4) for different durations. *T. sacculifer* (red squares) shows a fractionation of $\delta^{11}B$ after 6 hours leached in pH 4 whilst *G. ruber ss* shows no response after 6 and 10 hours. Dissolution tests on *G. ruber* was conducted twice on different sample set and for different maximum duration (6 hours, black open circles; and 10 hours, black filled circles).

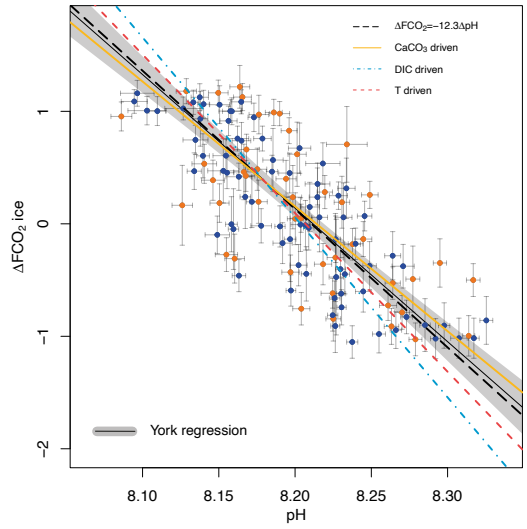

pH uncertainty from $\delta^{11}B$ borate only (2σ):
ΔF/ΔpH= - 12.4 ± 0.3 W/m2
mswd=6.07

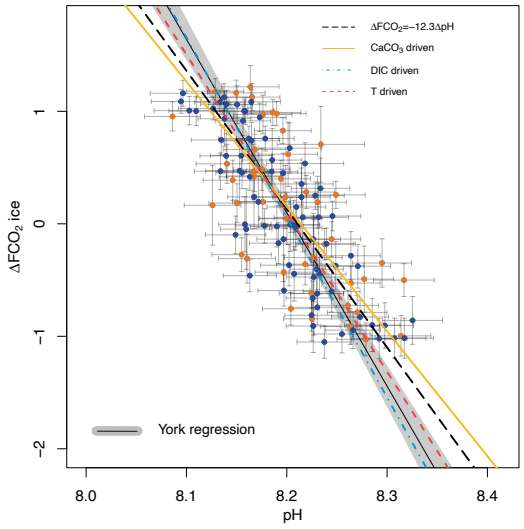

pH uncertainty from Monte Carlo simulation (2σ):
ΔF/ΔpH= - 15.4 ± 0.8 W/m²
mswd=1.09

Figure S7. Effect of pH uncertainty on the York regression between ΔFCO_2 and pH. The goodness of fit MSWD is improved when using the fully propagated pH uncertainty (from Monte Carlo simulation).

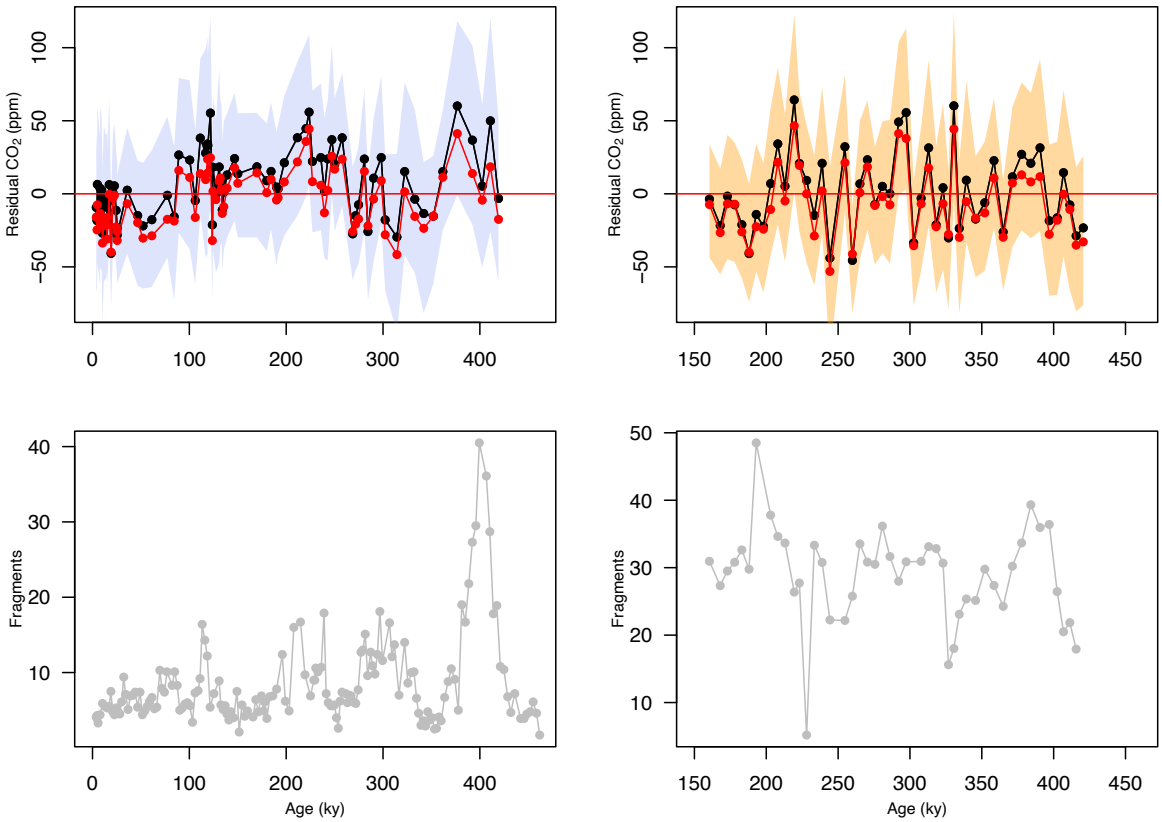

Figure S8. Comparison of CO_2 offset (or residual, δ^{11}B-derived CO_2 minus ice core CO_2) for CO_2 calculated with original SST (black line) or with SST including a pH correction (red line). Bottom row is the fragmentation index for each core location (left ODP Site 999, right ODP Site 871).

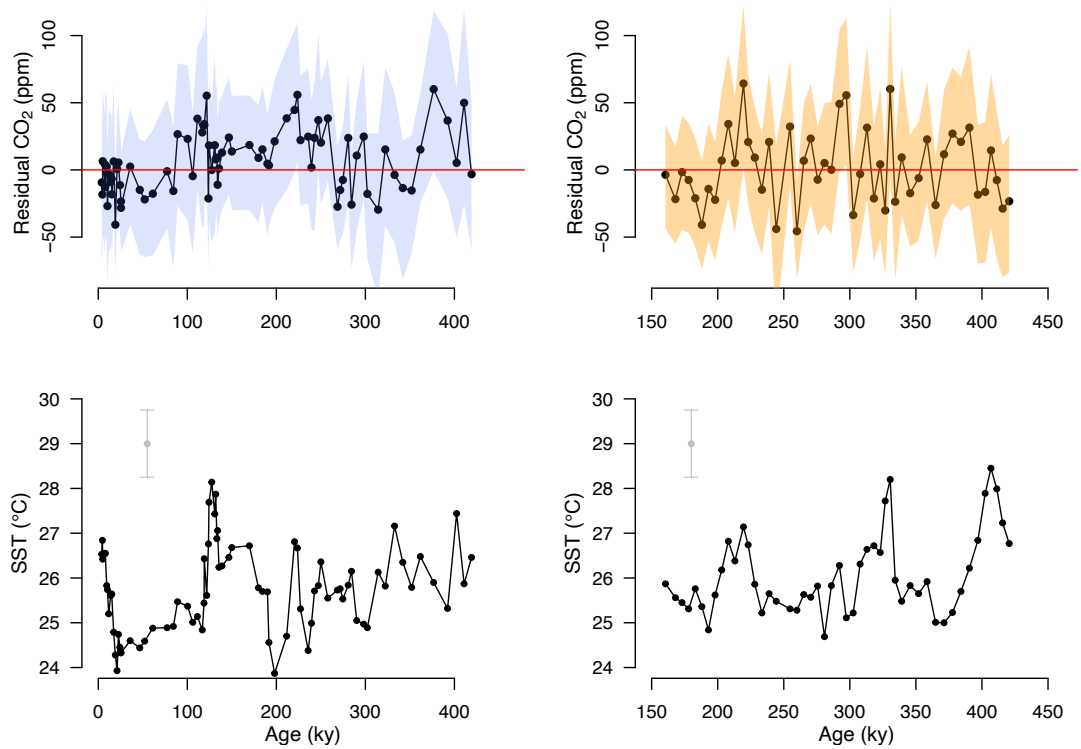

Figure S9. CO_2 offset (δ^{11}B-derived CO_2 minus ice core CO_2) compared to Mg/Ca-derived sea surface temperature of *G. ruber* (left ODP Site 999, right ODP Site 871). Periods of high CO_2 offset do not coincide with anomalous cold temperature recorded by *G. ruber*, ruling out upwelling and CO_2 disequilibrium as a cause of CO_2 offsets.

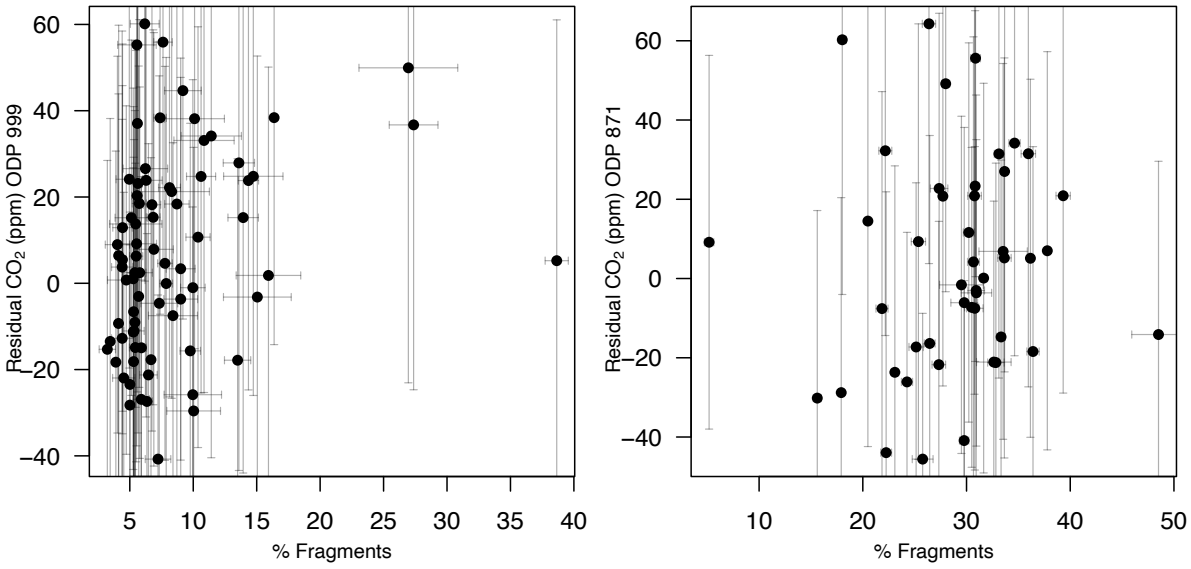

Figure S10. Crossplot of CO_2 residual (difference between CO_2 from ice cores and calculated from δ^{11}B) and fragment counts at site 999 (left) and 871 (right). Fragmentation index at site 999 (Schmidt et al. 2006) are interpolated from δ^{11}B-derived CO_2. Fragmentation index and δ^{11}B-derived CO_2 are from the same sample at site 871. Ice core CO_2 data are interpolated from δ^{11}B-derived CO_2 at both sites.

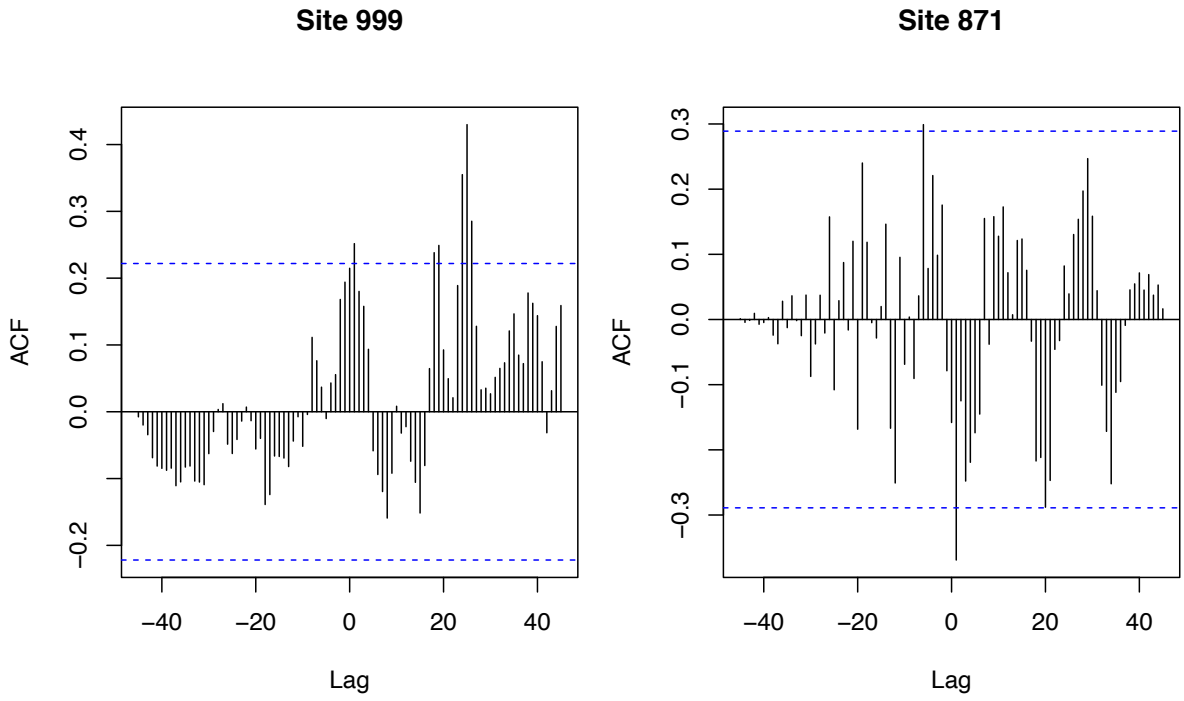

Figure S11. Cross-corelation function of CO_2 offset and fragmentation index for site 871 and 999. Negative (positive) lags mean that CO_2 offsets lead (lag) fragmentation index. The blue dotted lines are uncertainties, the values beyond which the autocorrelation (ACF) is significant. Whilst 6 values of ACF are outside uncertainty at site 999 and 2 values at site 871, most ACF values are within uncertainty and argue in favour of no correlation between CO_2 offset and fragmentation index.

Supplementary information S12. Relationship between pH, DIC and TA.

Dissolved inorganic carbon DIC and total alkalinity TA, are defined by the following, with [X] the concentration of compound X.

$$DIC = [CO_2] + [HCO_3^-] + [CO_3^{2-}] \text{ (eq 1a)}$$

$$TA = [HCO_3^-] + 2[CO_3^{2-}] + [B(OH)_4^-] + [OH^-] - [H^+] + minor\ compounds \text{ (eq 2a)}$$

At pH 8.1 in seawater CO_2 concentrations is small, such as equation (1a) can be approximated to:

$$DIC = [HCO_3^-] + [CO_3^{2-}] \text{ (eq 1b)}$$

TA can also be approximated by the carbonate alkalinity such as:

$$TA = [HCO_3^-] + 2[CO_3^{2-}] \text{ (eq 2b)}$$

By combining (eq1b) and (eq2b), we obtain:

$$TA - DIC = [CO_3^{2-}] \text{ (eq3)}$$
$$2DIC - TA = [HCO_3^-] \text{ (eq4)}$$

Now considering the equilibrium constants of carbonate compounds in seawater from the following chemical reactions (K_1 and K_2 are the equilibrium constants):

$$CO_2 + H_2O \Leftrightarrow [HCO_3^-] + [H^+] \ (K_1)$$
$$[HCO_3^-] \Leftrightarrow [CO_3^{2-}] + [H^+] \ (K_2)$$

$$\text{With } K_1 = \frac{[HCO_3^-][H^+]}{[CO_2]} \ (\text{eq5})$$

$$K_2 = \frac{[CO_3^{2-}][H^+]}{[HCO_3^-]} \ (\text{eq6})$$

It follows from (eq6), (eq3) and (eq4):

$$[H^+] = \frac{K_2(2DIC - TA)}{TA - DIC} \ (\text{eq7})$$

As pH is related to [H+], any change in alkalinity for a given pH, is compensated by a change in DIC.

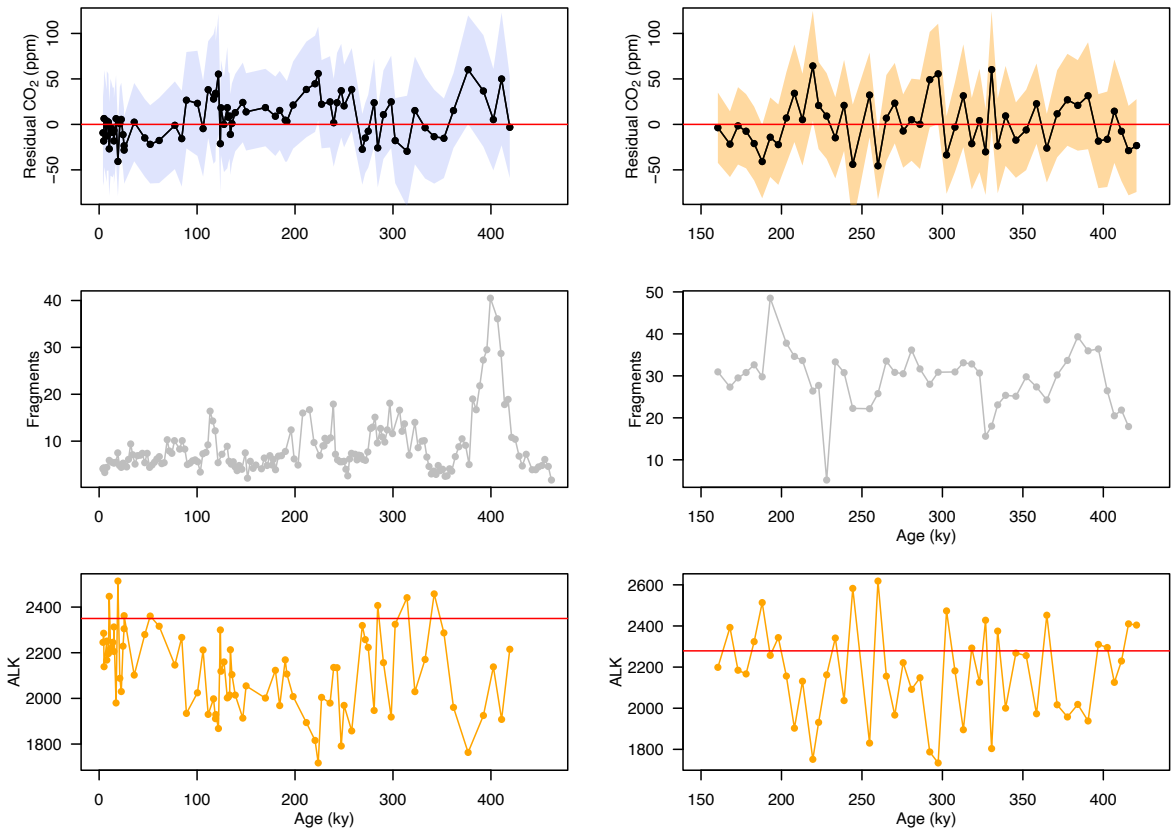

Figure S13. Left column: ODP Site 999, right column: ODP Site 871. Alkalinity (ALK, µmol/kg) change calculated from δ^{11}B-derived pH and ice core CO_2. The red line is the modern alkalinity values at each core site. If CO_2 offsets were only produced by alkalinity change, it would require an alkalinity change of up to 500 µmol/kg, a value beyond any estimated changes over the late Pleistocene (Hönisch et al., 2009, Cartapanis et al., 2018).

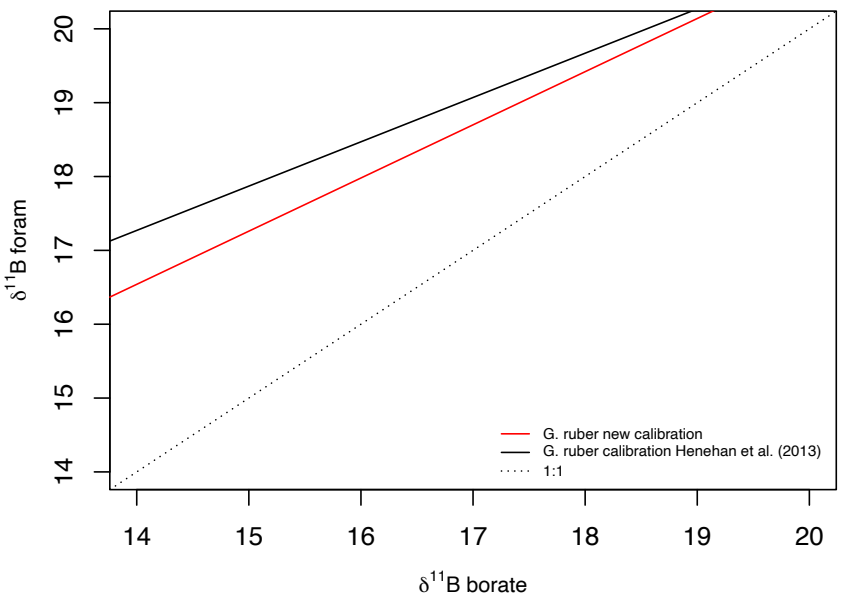

Figure S14. Calibration $\delta^{11}B_{foram\text{-}borate}$ of Henehan et al. (2013) (black line) and optimised calibration of this study (red line), showing a steeper slope for the new optimised calibration.

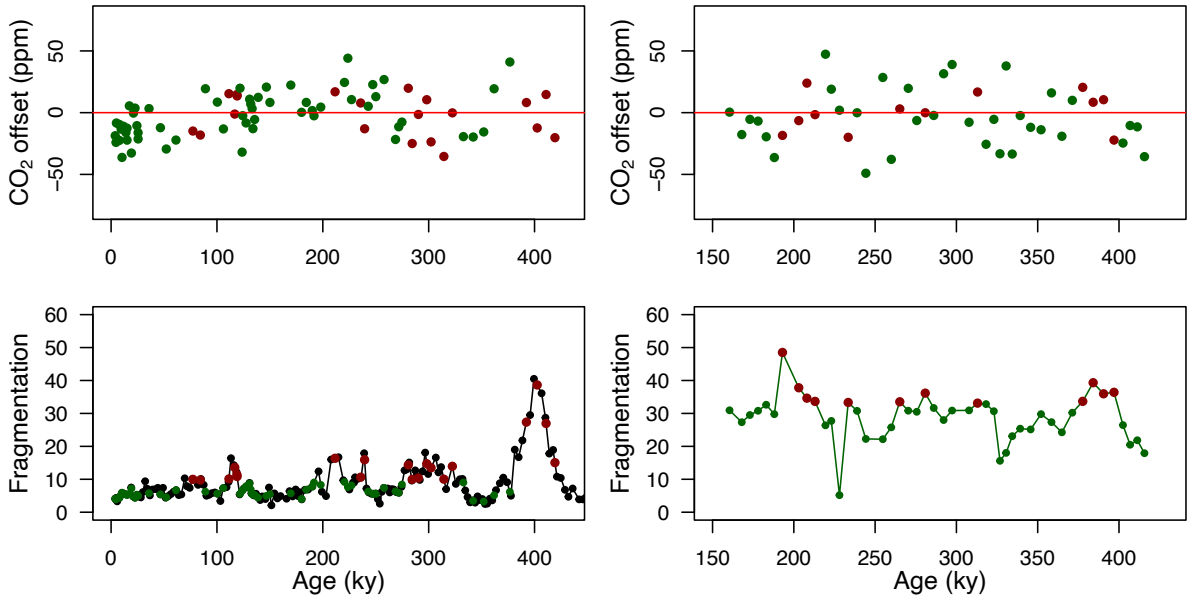

Figure S15. Left column: ODP Site 999, right column: ODP Site 871. CO_2 offset (coloured dots, defined as $\delta^{11}B$-derived CO_2 minus ice core CO_2) with optimised borate-foram $\delta^{11}B$ calibration. Lower panels: fragmentation index. Red dots in the lower panels are the fragments above the upper quartile (and corresponding CO_2 in the upper panel, red dots). Green dots represent periods of low fragments below the upper quartile (and corresponding CO_2 in the upper panel, green dots).